CHIRALITY 23:768–778 (2011)

Stereodynamics and Absolute Configuration of Stereolabile Atropisomers in 2,2-Dimethyl-1-aryl-1-indanols

DANIELE CASARINI,[1]* MICHELE MANCINELLI,[2] ANDREA MAZZANTI,[2]* AND FRANCESCA BOSCHI[2,3]

[1]*Department of Chemistry, University of Basilicata, via dell'Ateneo Lucano 10, Potenza 85100, Italy*
[2]*Department of Organic Chemistry "A. Mangini", University of Bologna, viale Risorgimento 4, Bologna 40136, Italy*
[3]*COMECER SpA, via Emilia Ponente 390, Castel Bolognese (RA) 48100, Italy*

Contribution to the Carlo Rosini Special Issue

ABSTRACT We describe herein the investigation of the stereodynamic processes occurring in a series of 1-aryl-2,2-dimethylindanols, by dynamic NMR. When the aryl moiety is a mesityl or a 2-methyl-1-naphthyl, the rotational barrier exceeds the 25 kcal/mol, so that stable atropisomers are observed. In two cases, all the chiral-atropisomeric species have been separated by enantioselective HPLC, and the comparison between theoretical and experimental electronic circular dichroism spectra allowed the absolute configuration assignment of all the isolated species to be obtained. *Chirality 23:768–778, 2011.*

KEY WORDS: indanols; dynamic NMR; enantioselective HPLC; electronic circular dichroism; DFT calculations

INTRODUCTION

Over the past several years, we have been using dynamic NMR spectroscopy to investigate the conformations and the stereomutation processes occurring in aryl alcohols derivatives.[1–4] In combination with these studies, we get intrigued in the investigation of 1-aryl-1-indanol derivatives, because a large number of bioactive and pharmaceutically interesting molecules contain the indanyl moiety[5–8] in the framework. In contrast to this, only little information is available in the literature about the conformational preferences of the aryl substituents and their effect on the chirooptical properties.

MATERIALS AND METHODS

General

All the solvents were dried over sodium/benzophenone and were distilled just before the use, once the mixture had turned to a persistent blue color. The 2,2-dimethyl-1-indanone was prepared according to the literature,[9,10] whereas the other reagents were of commercial grade (purity > 98%) and used without any further purification. The analytical TLC was performed on silica gel plates Merck 60 F 254, and the preparative purification was carried out on a chromatography column with silica gel Merck 60 (80–230 mesh). Analytical samples were obtained by semipreparative HPLC using a Waters Delta-600 pump and a Waters 2487 UV-detector. A Phenomenex Luna C18(2), 250 mm × 20 mm, 10-μm column was routinely used for the purifications.

3-Methoxybromomesitylene

A solution of 2,4,6-trimethylphenol (20 mmol) in 5 ml of THF was dropped in 20 min to a suspension of NaH 90% (22 mmol) in 40 ml of THF kept under N_2 and cooled at 5°C. The mixture was stirred as long as the gas evolution was completed, and then methyl sulfate (25 mmol) was added. After 1 h at room temperature, the reaction resulted completed, and it was quenched by adding 10 ml of water. THF was removed at reduced pressure, and the residue was extracted with ether. The collected organic layers were dried, the solvent removed, and the crude was dissolved in CH_2Cl_2 and reacted with bromine following a known procedure.[11]

^{1}H NMR ($CDCl_3$, 300 MHz) δ 2.23 (3H, s, *Me*), 2.34 (3H, s, *Me*), 2.38 (3H, s, *Me*), 3.69 (3H, s, O*Me*), 6.94 (1H, s, CH). ^{13}C NMR ($CDCl_3$, 75.5 MHz) δ 15.8 (CH_3), 16.8 (CH_3), 23.3 (CH_3), 60.1 (OCH_3), 125.1 (Cq), 129.3 (Cq), 130.0 (CH), 131.3 (Cq), 133.5 (Cq), 155.2 (Cq).

General Procedure for the Synthesis of the 2,2-Dimethyl-1-aryl-1-indanols (1-7)

n-BuLi 1.6 M in *n*-hexane (2.5 mmol) was added in 15 min to a solution of the appropriate aryl halide (2.5 mmol in 25 ml of dry THF), cooled to −80°C and under N_2. The mixture was allowed to react for 20 min, and then a solution of 2,2-dimethyl-1-indanone (2.5 mmol in 5 ml of dry THF) was added, and the temperature was allowed to rise slowly at 30°C. After checking by GC-MS, the end of the reaction, 40 ml of H_2O was added. The mixture was extracted with ether, and the collected organic layers were dried. Then, the solvent was removed, and the crude was purified by chromatography on a silica-gel column eluted with petroleum ether/acetone 9:1 Analytically pure samples were obtained by semipreparative HPLC on a C18 column.

1-(3,5-Dimethylphenyl)-2,2-dimethyl-2,3-dihydro-1H-inden-1-ol (1). ^{1}H NMR ($CDCl_3$, 600 MHz) δ 0.65 (3H, s, *Me*), 1.20 (3H, s, *Me*), 1.85 (1H, s, *OH*), 2.30 (6H, s, 2*Me*), 2.72 (1H, AB d, J = 15.5Hz, CH_2), 2.99 (1H, AB d, J = 15.5 Hz, CH_2), 6.92 (1H, s, Ph), 6.94 (2H, br s, Ph), 7.21 (1H, d, J = 7.2 Hz), 7.24 (1H, m), 7.30 (2H, m). ^{13}C NMR ($CDCl_3$, 150.8 MHz) δ 21.5 ($2CH_3$), 22.0 (CH_3), 26.4 (CH_3), 45.4 (CH_2), 48.3 (Cq), 88.0 (Cq), 124.8 (CH), 125.2 (2CH), 125.3 (CH), 126.7 (CH), 128.2 (CH), 128.6 (CH), 136.8 (2Cq), 141.9 (Cq), 143.5 (Cq), 147.7 (Cq). HRMS (ESI-FT-ICR) calcd for $C_{19}H_{21}O$ $[M\text{-}H]^-$ 265.15979; found 265.15942.

1-(3,5-Dimethylbenzyl)-2,2-dimethyl-2,3-dihydro-1H-inden-1-ol (2). ^{1}H NMR ($CDCl_3$, 600 MHz) δ 0.96 (3H, s, *Me*), 1.26 (3H, s, *Me*), 1.85 (1H, s, *OH*), 2.21 (6H, s, 2*Me*), 2.63 (1H, AB, J = 15.5Hz, CH_2Ph), 2.67 (1H, AB, J = 15.5Hz, CH_2), 2.78 (1H, AB, J = 15.5 Hz, CH_2), 2.93 (1H, AB, J = 15.5Hz, CH_2Ph), 6.37 (1H, d, J = 7.5Hz), 6.49 (2H, s, Ph), 6.84 (1H, s, Ph), 6.95 (1H, m), 7.14 (2H, m). ^{13}C NMR

Additional Supporting Information may be found in the online version of this article.

Contract grant sponsors: University of Basilicata (Potenza); MIUR-PRIN 2008, Rome; University of Bologna; Contract grant numbers: RFO 2008, RFO 2009.

*Correspondence to: Andrea Mazzanti, Department of Organic Chemistry "A. Mangini," University of Bologna, viale Risorgimento 4, Bologna 40136, Italy. E-mail: mazzand@ms.fci.unibo.it

Received for publication 23 February 2011; accepted in revised form 13 May 2011; Accepted 17 May 2011
DOI: 10.1002/chir.20988
Published online 18 August 2011 in Wiley Online Library (wileyonlinelibrary.com).

($CDCl_3$, 150.8 MHz) δ 21.2 ($2CH_3$, Ph), 22.2 (CH_3), 24.1 (CH_3), 41.9 (*CH_2*Ph), 45.0 (CH_2), 47.8 (Cq), 85.0 (Cq), 124.6 (CH), 125.0 (CH), 125.1 (CH), 127.5 (CH), 127.8 (CH, Ph), 129.0 (2CH, Ph), 136.9 (Cq), 136.9 (2Cq, Ph), 140.3 (Cq, Ph), 146.2 (Cq). HRMS (ESI-FT-ICR) calcd for $C_{20}H_{23}O$ $[M\text{-}H]^-$ 279.17544; found 279.17514.

1-Mesityl-2,2-dimethyl-2,3-dihydro-1H-inden-1-ol (3). ^1H NMR ($CDCl_3$, 600 MHz) δ 1.00 (3H, s, *Me*), 1.35 (3H, s, *Me*), 1.40 (3H, s, *Me*), 1.82 (1H, s, *OH*), 2.23 (3H, s, *Me*), 2.66 (3H, s, *Me*), 2.94 (1H, AB d, J = 16.2 Hz, *CH_2*), 2.97 (1H, AB d, J = 16.2 Hz, *CH_2*), 6.65 (1H, s, Ph), 6.92 (1H, s, Ph), 7.16–7.23 (3H, m), 7.26 (1H, dt, J = 7.2; 1.4 Hz). ^{13}C NMR ($CDCl_3$, 150.8 MHz) δ 20.4 (CH_3), 23.5 (CH_3), 25.8 (CH_3), 27.2 (CH_3), 27.9 (CH_3), 48.6 (Cq), 49.0 (CH_2), 90.8 (Cq), 124.9 (CH), 125.2 (CH), 127.3 (CH), 128.3 (CH), 130.9 (CH), 131.9 (CH), 135.3 (Cq), 136.2 (Cq), 138.6 (Cq), 139.1 (Cq), 141.3 (Cq), 151.0 (Cq). HRMS (ESI-FT-ICR) calcd for $C_{20}H_{23}O$ $[M\text{-}H]^-$ 279.17544; found 279.17557.

1-(3-Methoxy-2,4,6-trimethylphenyl)-2,2-dimethyl-2,3-dihydro-1H-inden-1-ol (4). Major Atropisomer (54%) ^1H NMR ($CDCl_3$, 600 MHz) δ 1.02 (3H, s, *Me*), 1.31 (3H, s, *Me*), 1.39 (3H, s, *Me*), 1.77 (1H, s, *OH*), 2.22 (3H, s, *Me*), 2.58 (3H, s, *Me*), 2.95 (2H, s, *CH_2*), 3.73 (3H, s, O*CH_3*), 6.64 (1H, s, Ar), 7.12 (1H, d, J = 7Hz, Ar), 7.16–7.22 (2H, m, Ar), 7.26 (1H, t, J = 7 Hz, Ar). ^{13}C NMR ($CDCl_3$, 150.8 MHz) δ 15.8 (CH_3), 17.4 (CH_3), 22.8 (CH_3), 27.4 (CH_3), 27.9 (CH_3), 48.4 (Cq), 49.5 (CH_2), 59.4 (OCH_3), 90.7 (Cq), 124.7 (CH), 125.5 (CH), 127.4 (CH), 128.3 (CH), 128.4 (Cq), 131.4 (Cq), 132.3 (Cq), 133.2 (CH), 141.2 (Cq), 141.3 (Cq), 151.0 (Cq), 156.4 (Cq).

Minor Atropisomer (46%) ^1H NMR ($CDCl_3$, 600 MHz) δ 1.00 (3H, s, *Me*), 1.35 (3H, s, *Me*), 1.37 (3H, s, *Me*), 1.90 (1H, s, *OH*), 2.23 (3H, s, *Me*), 2.62 (3H, s, *Me*), 2.94 (1H, J_{AB} = 16 Hz, *CH_2*), 3.01 (1H, J_{AB} = 16 Hz, *CH_2*), 3.54 (3H, s, O*CH_3*), 6.92 (1H, s, Ar), 7.12 (1H, d, J = 7 Hz, Ar), 7.16–7.22 (2H, m, Ar), 7.26 (1H, t, J = 7Hz, Ar). ^{13}C NMR ($CDCl_3$, 150.8 MHz) δ 15.5 (CH_3), 15.8 (CH_3), 25.4 (CH_3), 27.2 (CH_3), 28.1 (CH_3), 48.2 (Cq), 48.9 (CH_2), 59.4 (OCH_3), 90.7 (Cq), 124.8 (CH), 125.0 (CH), 127.3 (CH), 128.1 (CH), 128.2 (Cq), 129.9 (Cq), 132.4 (CH), 134.4 (Cq), 140.6 (Cq), 141.1 (Cq), 151.1 (Cq), 155.4 (Cq). HRMS (ESI-FT-ICR) calcd for $C_{21}H_{25}O_2$ $[M\text{-}H]^-$ 309.18600; found 309.18568.

1-(Benzo[b]thiophen-7-yl)-2,2-dimethyl-2,3-dihydro-1H-inden-1-ol (5). ^1H NMR ($CDCl_3$, 600 MHz) δ 0.78 (3H, s, *Me*), 1.35 (3H, s, *Me*), 2.29 (1H, s, *OH*), 2.79 (1H, AB d, J = 15.5Hz, *CH_2*), 3.02 (1H, AB d, J = 15.5Hz, *CH_2*), 6.64 (1H, d, J = 7.5Hz, Ar), 7.21 (1H, t, J = 7.5Hz, Ar), 7.27 (2H, m, Ar), 7.33 (2H, m, Ar), 7.35 (1H, d, J = 5.6Hz; Ar), 7.48 (1H, d, J = 5.6Hz; Ar), 7.75 (1H, d, J = 7.6Hz; Ar). ^{13}C NMR ($CDCl_3$, 150.8 MHz) δ 22.2 (CH_3), 26.0 (CH_3), 45.2 (CH_2), 48.8 (Cq), 87.3 (Cq), 121.7 (CH), 122.1 (CH), 123.3 (CH), 123.8 (CH), 124.0 (CH), 124.5 (CH), 125.5 (CH), 126.9 (CH), 129.0 (CH), 139.6 (Cq), 139.7 (Cq), 142.9 (Cq), 146.7 (Cq), 148.2 (Cq). HRMS (ESI-FT-ICR) calcd for $C_{19}H_{17}OS$ $[M\text{-}H]^-$ 293.10056; found 293.10028.

2,2-Dimethyl-1-(naphthalen-1-yl)-2,3-dihydro-1H-inden-1-ol (6). Major Atropisomer (85%) ^1H NMR ($CDCl_3$, 600 MHz) δ 0.79 (3H, s, *Me*), 1.39 (3H, s, *Me*), 1.53 (1H, s, *OH*), 2.79 (1H, AB d, J = 15.5 Hz, *CH_2*), 2.87 (1H, AB d, J = 15.5 Hz, *CH_2*), 6.67 (1H, dd, J = 7.3; 1.2 Hz, Ar), 7.21 (1H, t, J = 7.5 Hz, Ar), 7.29–7.31 (3H, m, Ar), 7.34 (1H, m, Ar), 7.46 (1H, m, J = 8.5;1.5 Hz, Ar), 7.50 (1H, m, J = 8.5;1.5 Hz, Ar), 7.73 (1H, d, J = 8.0 Hz, Ar), 7.84 (1H, dd, J = 8.0; 1.5 Hz, Ar), 9.19 (1H, dd, J = 9.0, 0.8 Hz, Ar). ^{13}C NMR ($CDCl_3$, 150.8 MHz) δ 24.4 (CH_3), 26.9 (CH_3), 46.0 (CH_2), 49.8 (Cq), 92.3 (Cq), 124.2 (CH), 124.8 (CH), 124.9 (CH), 125.0 (CH), 125.1 (CH), 127.1 (CH), 127.5 (CH), 128.4 (CH), 128.6 (CH), 128.7 (CH), 129.4 (CH), 132.7 (Cq), 134.9 (Cq), 138.4 (Cq), 142.4 (Cq), 149.7 (Cq).

Minor Atropisomer (15%) ^1H NMR ($CDCl_3$, 600 MHz) δ 0.75 (3H, s, *Me*), 1.29 (3H, s, *Me*), 1.68 (1H, s, *OH*), 2.87 (1H, AB d, J = 15.5Hz, *CH_2*), 3.22 (1H, AB d, J = 15.5 Hz, *CH_2*), 7.01 (1H, d, J = 7.6 Hz, Ar), 7.06 (1H, m, Ar), 7.16 (1H, t, J = 7.3 Hz, Ar), 7.40 (1H, d, J = 8.5 Hz, Ar), 7.42 (1H, d, J = 8.5 Hz, Ar), 7.59 (1H, t, J = 8.0 Hz, Ar), 7.82 (1H, d, J = 8.0 Hz, Ar), 8.24 (1H, dd, J = 7.3; 1.2 Hz, Ar). ^{13}C NMR ($CDCl_3$, 150.8 MHz) δ 21.4 (CH_3), 28.3 (CH_3), 45.9 (CH_2), 49.8 (Cq), 92.3 (Cq), 123.9 (CH), 124.6 (CH), 125.0 (CH), 125.1 (CH), 125.4 (CH), 126.1 (CH), 126.7 (CH), 127.8 (CH), 128.1 (CH), 128.5 (CH), 128.8 (CH), 131.7 (Cq), 134.2 (Cq), 138.0 (Cq), 142.6 (Cq), 147.9 (Cq). HRMS (ESI-FT-ICR) calcd for $C_{21}H_{19}O$ $[M\text{-}H]^-$ 287.14414; found 287.14380.

2,2-Dimethyl-1-(2-methylnaphthalen-1-yl)-2,3-dihydro-1H-inden-1-ol (7). Major Atropisomer (70%) ^1H NMR ($CDCl_3$, 600 MHz) δ 1.06 (3H, s, *Me*), 1.55 (3H, s, *Me*), 1.61 (3H, s, *Me*), 2.18 (1H, s, *OH*), 3.02 (1H, AB d, J = 16.5 Hz, *CH_2*), 3.07 (1H, AB d, J = 16.5 Hz, *CH_2*), 7.08 (1H, d, J = 8.5 Hz, Ar), 7.17 (1H, d, J = 7.5 Hz, Ar), 7.25 (1H, t, J = 7.5 Hz, Ar), 7.26 (1H, m, Ar), 7.31 (1H, dt, J = 7.0;1.2 Hz, Ar), 7.40 (1H, dt, J = 6.5; 1.2 Hz, Ar), 7.45 (1H, m, J = 8.5; 6.5; 1.6 Hz, Ar), 7.63 (1H, d, J = 8.5Hz, Ar), 7.78 (1H, dd, J = 8.0;1.5Hz, Ar), 9.01 (1H, d, J = 8.8Hz, Ar). ^{13}C NMR ($CDCl_3$, 150.8 MHz) δ 24.2 (CH_3), 27.0 (CH_3), 28.0 (CH_3), 49.0 (CH_2), 49.0 (Cq), 91.5 (Cq), 124.2 (CH), 124.3 (CH), 125.0 (CH), 125.2 (CH), 127.5 (CH), 127.8 (CH), 128.1 (CH), 128.4 (CH), 129.9 (CH), 131.0 (CH), 133.5 (Cq), 133.7 (Cq), 134.4 (Cq), 138.2 (Cq), 141.3 (Cq), 151.0 (Cq).

Minor Atropisomer (30%) ^1H NMR ($CDCl_3$, 600 MHz) δ 1.00 (3H, s, *Me*), 1.50 (3H, s, *Me*), 1.68 (1H, br s, *OH*), 2.90 (3H, s, *Me*), 3.00 (1H, AB d, J = 16.5Hz, *CH_2*), 3.17 (1H, AB d, J = 16.5Hz, *CH_2*), 6.77 (1H, d, J = 7.5Hz, Ar), 6.86 (1H, m, J = 8.5;6.7;1.5Hz, Ar), 7.05 (1H, d, J = 9.0Hz, Ar), 7.06 (1H, t, J = 7.5Hz, Ar), 7.18 (1H, t, J = 7.2Hz, Ar), 7.28 (1H, dt, J = 7.5;1.5Hz, Ar), 7.34 (1H, d, J = 7.7Hz, Ar), 7.36 (1H, d, J = 8.5 Hz, Ar), 7.65 (1H, d, J = 8.5 Hz, Ar), 7.68 (1H, dd, J = 8.0; 1.6 Hz, Ar). ^{13}C NMR ($CDCl_3$, 150.8 MHz) δ 24.5 (CH_3), 26.3 (CH_3), 28.5 (CH_3), 46.0 (Cq), 47.5 (CH_2), 91.2 (Cq), 123.3 (CH), 123.6 (CH), 125.2 (CH), 125.6 (CH), 127.1 (CH), 127.9 (CH), 128.2 (2CH), 128.3 (CH), 132.1 (CH), 132.6 (Cq), 132.9 (Cq), 136.4 (Cq), 138.0 (Cq), 140.7 (Cq), 151.4 (Cq). HRMS (ESI-FT-ICR) calcd for $C_{22}H_{21}O$ $[M\text{-}H]^-$ 301.15979; found 301.15948.

NMR Spectroscopy

The spectra were recorded at 600 MHz for ^1H and 150.8 MHz for ^{13}C. The assignments of the ^1H and ^{13}C signals were obtained by bi-dimensional experiments (COSY, edited-*g*HSQC,[12,13] and gHMBC[14] sequences). The NOE experiments were obtained by means of the DPFGSE-NOE[15] sequence. To selectively irradiate the desired signal, a 20-Hz wide-shaped pulse was calculated with a refocusing-SNOB shape[16] and a pulse width of 92.5 ms. Mixing time was set to 1.8 s. The samples for obtaining spectra at temperatures lower than −100°C were prepared by connecting to a vacuum line the NMR tubes containing the compound and a small amount of C_6D_6 (for locking purpose), and condensing therein the gaseous CHF_2Cl and $CHFCl_2$ (4:1 v/v) under cooling with liquid nitrogen. The tubes were subsequently sealed in vacuum and introduced into the precooled probe of the spectrometer. The temperature calibrations were performed before the experiments, using a Cu/Ni thermocouple immersed in a dummy sample tube filled with isopentane, and under conditions as nearly identical as possible. The uncertainty in the temperatures was estimated from the calibration curve to be ±2°C. The line shape simulations were performed by means of a PC version of the QCPE program DNMR 6 n° 633, Indiana University, Bloomington, IN.

Calculations

Geometry optimization was carried out at the B3LYP/6-31G(d) and CAM-B3LYP/6-31G(d) level by means of the Gaussian 03 and Gaussian 09 series of programs.[17,18] The standard Berny algorithm in redundant internal coordinates and default criteria of convergence were used. The harmonic vibrational frequencies were calculated for all the stationary points. For each optimized ground state, the frequency analysis showed the absence of imaginary frequencies, whereas each transition state showed a single imaginary frequency. Visual inspection of the corresponding normal mode was used to confirm that the correct transition state had been found. If not explicitly indicated, the reported energy values represent the total electronic energies. In general, these give the best fit with experimental Dynamic-NMR data.[19,20] This approach avoids artifacts that might result from the inevitably ambiguous choice of an adequate reference temperature, and from the idealization of low-fre-

quency vibrators as harmonic oscillators (very important in the present cases, where about one third of the calculated frequencies fall below the 500–600 cm^{-1} range). TD-DFT calculations of **3** and **4** were obtained at the CAM-B3LYP/6-311++G(2d,p)//CAM-B3LYP/6-31G(d) level. TD-DFT calculations of **7** were obtained at the CAM-B3LYP/6-311+G(d,p)//B3LYP/6-31G(d) level. To cover the 170–400 nm range, 50–75 transitions were calculated. The electronic circular dichroism (ECD) spectra were then obtained by applying a 0.55 eV Gaussian band-shape.[21]

Enantioselective HPLC Separation and ECD Spectra

The analytic separation of the racemic mixtures of compounds **3**, **4**, and **7** was achieved at 25°C on a DAICEL Chiralcel AD-H 250 mm × 4.6 mm column, at a flow rate of 1.0 mL/min, using hexane/iPr-OH 90:10 v:v as eluent. Semipreparative separations were obtained on a semipreparative DAICEL Chiralcel AD-H 250 mm × 21.2 mm at a flow rate of 20 ml/min, using the same eluent. In the case of compound **4**, a Phenomenex LUX Amylose-2 (250 mm × 10 mm, 5 μm, 4 ml/min, hexane/iPr-OH 98:2 v:v) was also used. UV detection was fixed at 210 nm. UV absorption spectra were recorded at 25°C in acetonitrile on the racemic mixtures, in the 190–400 nm spectral region. The cell path length was 0.1 cm, concentration was 1.0–1.2 × 10^{-4} mol/L. ECD spectra were recorded at 25°C in acetonitrile solutions, with the same path lengths and concentrations used for UV spectra, in the range 190–400 nm; reported Δε values are expressed as L/mol/cm.

X-Ray Diffraction

Crystals of compound **6** suitable for X-ray analysis were obtained by slow evaporation of an hexane solution. Molecular formula: $C_{21}H_{20}O$, M_r = 288.37, monoclinic, space group $P2_1/c$ (No. 14), a = 8.823(4), b = 8.564(3), c = 20.207(8) Å, β = 93.274(5), V = 1524.3(11) $Å^3$, T = 298(2) K, Z = 4, ρ_c = 1.257 g/cm^3, $F(000)$ = 616, graphite-monochromated $Mo_{K\alpha}$ radiation (λ = 0.71073 Å), $\mu(Mo_{K\alpha})$ = 0.075 mm^{-1}, colorless brick (0.6 × 0.4 × 0.4 mm^3), empirical absorption correction with SADABS (transmission factors: 0.9706–0.9563), 2400 frames, exposure time 10 s, $2.58 \le \theta \le 28.63$, $-11 \le h \le 11$, $-11 \le k \le 11$, $-27 \le l \le 26$, 16301 reflections collected, 3673 independent reflections (R_{int} = 0.0556), solution by direct methods (SHELXS97) and subsequent Fourier syntheses, full-matrix least-squares on F_o^2 (SHELXTL 6.10), hydrogen atoms refined with a riding model except for the hydroxyl hydrogen that was experimentally localized and optimized. Data/restraints/parameters = 3673/0/205, $S(F^2)$ = 1.034, $R(F)$ = 0.0715, and $wR(F^2)$ = 0.1774 on all data, $R(F)$ = 0.0594 and $wR(F^2)$ = 0.1636 for 2910 reflections with $I > 2\sigma(I)$, weighting scheme $w = 1/[\sigma^2(F_o^2) + (0.1130P)^2 + 0.2301P]$ where $P = (F_o^2 + 2F_c^2)/3$, largest difference peak and hole 0.438 and −0.268 e/$Å^3$*

RESULTS AND DISCUSSION

The 1-arylindanols of Chart 1 resemble the sterically hindered tertiary aryl carbinols that are known to display hindered rotation around the Cq-Ar bond when the two remaining substiuents are sufficiently large.[22,23] In the present case, the two substituents are linked together in the rigid indanyl core, and therefore, the conformational freedom is further reduced. For this reason, these aryl indanols exhibit a restricted rotation about the C(OH)–Ar bond because of the steric interaction in the rotational transition state between the ortho substituents of the 1-aryl moiety and the geminal

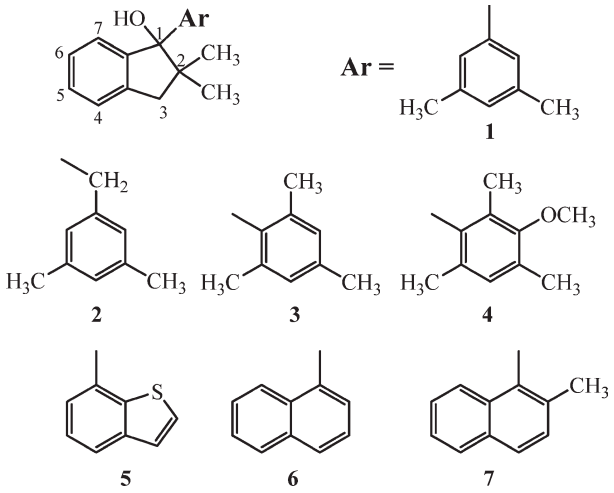

Chart 1. Chemical formula of aryl-indanols 1-7.

methyl groups that protrude from the 2-position on the indane ring.

The lack of symmetry due to the chiral carbon on the indanyl structure implies a C_1 symmetry in all the investigated molecules, even when the rotation around the Cq-Ar bond is rapid in the NMR time scale. Furthermore, the chiral center makes diastereotopic the two adjacent geminal methyls as well as the methylenic hydrogens on the same ring.[24] For this reason, the ^1H and ^{13}C variable temperature spectra (at 600 and 150.8 MHz, respectively) can monitor the aryl rotation in compound **1** only by the splitting of the *ortho*-hydrogens and *meta*-methyls in the phenyl ring. The local C_2 symmetry axis of the 3,5-dimethylphenyl ring implies that when the rotation is frozen the groups that do not lie on such axis experience a different environment and the corresponding NMR signals split into two equally intense lines.

On cooling, a sample of **1** in $CDFCl_2$ below −30°C broadening of the *ortho*-hydrogens and of the *meta*-methyl signals is observed as a consequence of the restricted rotation of the phenyl ring that generates two identical conformers (topomerization). In the ^1H spectrum, the signals reach the coalescence point at −53°C and sharpen again at −77°C into a 1:1 ratio (Fig. 1) with a separation of 89 Hz (554 Hz in the ^{13}C spectrum, Supporting Information Fig. S1). The line shape simulation allowed the determination of the rate constant for the dynamic process at various temperatures; from these values, a rotational barrier of 10.4 ± 0.2 kcal/mol was derived in both the ^1H and ^{13}C simulated spectra.

On further cooling below −100°C, the signals of the phenyl moiety remain sharp and keep the same shift, whereas those belonging to the indanyl framework broaden and change their chemical shift with the temperature (Fig. 2). However, below −120°C even the phenyl signals begin to broaden, so that at −150°C all signals are divided approximately with a 70:30 ratio, and the spectrum exhibits a complex pattern of overlapped signals. This dynamic behavior can be attributed to the slowing down of the flipping in the five-membered ring that generates two diastereomeric conformers. Unfortunately below −150°C, the solute precipitated

*Crystallographic data (excluding structure factors) for the structure reported in this paper have been deposited with the Cambridge Crystallographic Data Centre as supplementary publication no. CCDC-813948. Copies of the data can be obtained free of charge on application to CCDC, 12 Union Road, Cambridge CB21EZ, UK. Fax: (+44) 1223-336-033; e-mail: deposit @ccdc.cam. ac.uk.

preventing from the observation of the complete ^{1}H signal splitting. A rough estimation, based on the coalescence point (about −130°C), indicates a value of 6.0 ± 0.4 kcal/mol for the energy barrier of this process.

DFT calculations showed that in the indanyl frame the five-membered ring is not planar and the CMe_2 carbon does not lie on the same plane of the phenyl. Because of the presence of the asymmetric carbon in position 1, the two possible positions of the CMe_2 moiety (i.e., over or under the plane of the phenyl) correspond to two diastereomeric conformations (see Fig. 3) that can be named as "*syn*" when the $C(Me_2)$ is on the same side of the hydroxyl group, and "*anti*" when the edge of the envelope is on the other side. The calculations (at the B3LYP/6-31G(d) and CAM-B3LYP/6-31G(d) levels) indicate that both conformations should be populated, their energy difference being 0.8 kcal/mol after zero point energy correction (ZPE). These two conformational diastereoisomers can exchange by the flipping of the five-membered ring, through a transition state where the cycle is planar (see Fig. 3). This transition state has a calculated barrier of 4.5 kcal/mol, in reasonable agreement with the experimental data. The same calculations estimate a barrier of 9.6 kcal/mol for the rotation of the 3,5-dimethylphenyl, again in good agreement with the experiment. The four stationary points found by DFT were then recalculated as single point energies at the ab initio CISD/6-31G(d) level, to verify if an higher level of calculation could provide a better fit with the experimental data. The results were almost identical with that obtained with DFT regarding the energy difference between the two ground states (0.9 kcal/mol). On the contrary, the transition state energies were higher with respect to the DFT data and matched very well the experimental data (10.5 and 7.0 kcal/mol for the aryl-rotation and for the ring inversion, respectively). These results show that the CISD approach could provide slightly better data at the price of very large computational times. On the other hand, the DFT approach should be considered suitable to tackle the conformation analysis of the present set of molecules because of its fairly good accuracy coupled with a reasonable computational cost.[†]

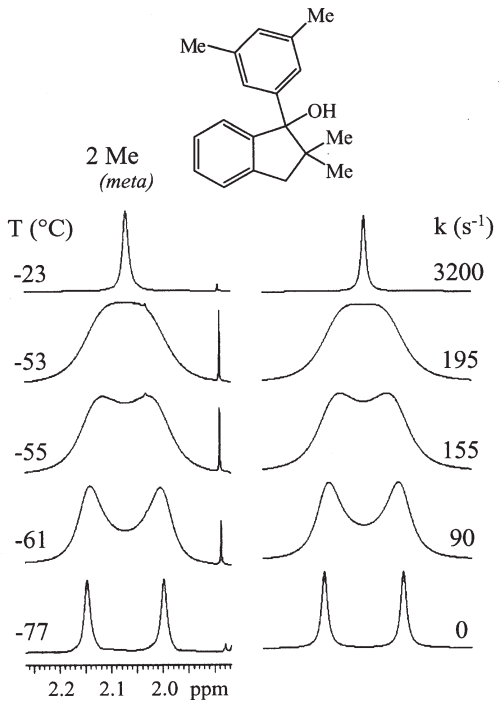

Fig. 1. ^{1}H NMR spectra (600 MHz in $CDFCl_2$) of compound **1**. (Left) experimental traces at various temperatures of the *meta*-methyls of the phenyl ring. (Right) line shape simulations and rate constants (*k*) at the same temperatures.

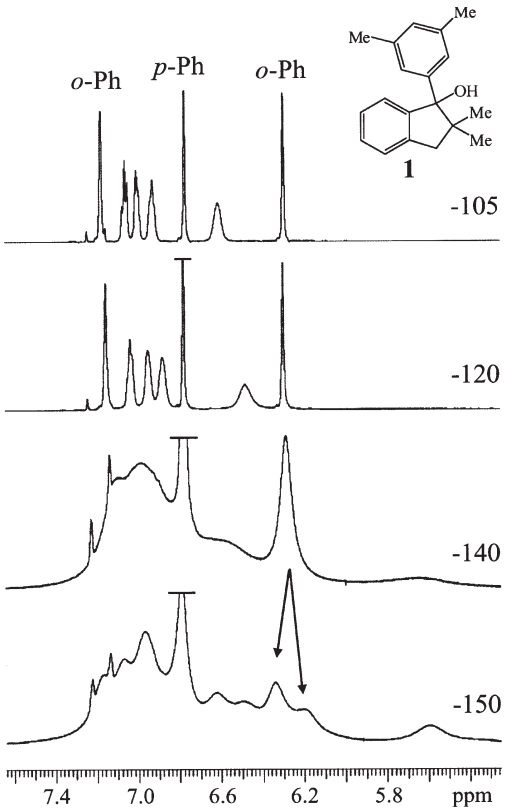

Fig. 2. ^{1}H NMR spectra (600 MHz in $CDFCl_2$) of the aromatic zone of compound **1**. At −150°C all the signals are split approximately in a 70:30 ratio (arrows).

The barriers to rotation observed in the 2,2-dimethylindanols (**1**–**7**) are largely influenced by the bulkiness of the aryl substituent[25,26],[‡] as shown in Table 1.

When the *ortho*-hydrogens of the aryl group are replaced by methyls (compound **3**), the steric hindrance, and consequently, the barrier increases so much that the mesityl rotation is already locked at 25°C, as deduced by the ^{1}H spectrum where the *ortho*-methyls and the *meta*-hydrogens show pairs of sharp singlets separated by 750 and 160 Hz, respec-

[†]A single point energy CISD/6-31G(d) calculation on compound **1** takes about 16 h on a 8-cores job running on Xeon X7355 processors @ 2.93 GHz, with a scratch file of about 32 Gbytes. CISD calculations scale roughly with N^6 (N being the number of the basis functions, that is, of the orbitals), so this approach would imply computational times close to a week when dealing with larger molecules like compound **5**, **6**, and **7**. On the other hand, an optimization with DFT and the subsequent frequency calculation usually takes 2–8 h.

[‡]The steric origin of the barrier to rotation is further supported by the fact that the insertion of a methylene between the indanyl and the phenyl, compound **2**, drastically reduces the barrier at about 6.0 kcal/mol (Supporting Information Figs. S2 and S3) in good agreement with the values measured in similar compounds.[25,26] Actually, the whole rotational process for **2** consists of two simultaneous rotational processes: indanyl–CH_2 and CH_2–Ph, which allow to better accommodate the phenyl bulkiness and thus facilitate the whole motion by reducing the steric interactions.

TABLE 1. Rotational barriers ($\Delta G^{\neq}$) for 1-aryl-2,2-dimethylindanols (1–7)

Cpd	Exp. sp/ap ratio	Calcd. sp/ap ratio	Exp $\Delta G^{\neq}$ (kcal/mol)	Calcd $\Delta E^{\neq}$ (kcal/mol)
1	Topomers	–	10.4	9.6,[a] 10.5[b]
			6.2 (inversion)	4.3,[a] 7.0[b]
2	Topomers	–	6.0	–
3	Topomers	–	>22.0	29.0[a]
4	54:46	52:48[a]	26.9_5	29.9[a]
5	96:4	97:3[d]	16.7	17.0[d]
6	89:11	81:19[c]	18.8	19.6[c]
7	70:30	66:34[c]	25.5	26.7[c]

[a]CAM-B3LYP/6–31G(d).
[b]CISD/6–31G(d)//B3LYP/6–31G(d).
[c]B3LYP/6–31G(d).
[d]CAM-B3LYP/6–311++G(2d,p).

tively. The huge separation between the methyl signals can be referred to the ring-current effect that shifts upfield the methyl (1.40 ppm) if it is oriented inward the indanyl moiety. Consequently, the phenyl must be nearly perpendicular to the aromatic part of the indane so that the second *ortho*-methyl results oriented toward the geminal methyls and shifted downfield to 2.66 ppm. These remarks are completely supported by NOE experiments (Fig. 4). Saturation of the methyl at 2.66 ppm yields a strong NOE on the *meta*-hydrogen at 6.92[§] and other significant NOE effects on the OH and both the geminal methyls at 1.00 and 1.35 ppm. On the contrary, the irradiation of the methyl at 1.40 ppm shows a strong NOE effect on the other *meta*-hydrogen at 6.65 ppm,[§] on the H7 of the indane at 7.2 ppm and on the methyl at 1.00 ppm, whereas no effect is observed on the OH signal. Finally, the irradiation of the methyl at 1.00 ppm show nearly equivalent NOEs on both the *ortho*-methyls proving that they are at similar distances. This implies that the mesityl and the indanyl moieties must adopt a propeller-like disposition (see Fig. 4).[27,28]

DFT calculations suggest that the ground state structure of compound **3** adopts a propeller-like disposition between the two aromatic rings. The energy difference between the two conformational diastereoisomers, generated by the different dispositions of the CMe_2 group, is very small (0.6 or 0.2_5 kcal/mol, if the free energy is considered), thus both conformations should be populated when the inversion of the five-membered ring is frozen. NOE data confirm that the most populated conformation corresponds to the lowest energy structure, where the OH and the CMe_2 are on the same side of the plane of the aromatic ring in the indane (*syn*). In this conformation, the distances (and thus the NOE enhancements) between the two geminal methyls of CMe_2 and between one of the latter with the two *ortho*-methyl of mesitilene are very similar, as experimentally observed (top trace in Fig. 4).

The calculations also suggest that the barrier for the five-membered ring inversion is considerably smaller (2.0 kcal/mol) with respect to that calculated in compound **1**. Taking into account the underestimation of the DFT calculations in the case of compound **1** (about 1.7 kcal/mol), the ring inversion barrier in compound **3** should be comprised in the 3.5–4.5 kcal/mol range, a barrier hardly observable by the dynamic NMR technique.[29–32] Low-temperature spectra of **3** down to −160°C did not show any further broadening ascribable to the slowdown of the ring inversion. The lowering of the barrier to the ring inversion could be due to the steric hindrance caused by the mesityl ring that flattens the envelope of the ring and rises the energy of the ground state, thus reducing the barrier.[¶]

When a sample of **3** was heated in $C_2D_2Cl_4$, the signals of the *ortho*-methyls remained sharp at all the temperatures and the large chemical shift separations resulted almost unchanged even at +140°C, confirming that the rotational barrier of the mesityl is larger than 22 kcal/mol and that it is too high to be handled by the Dynamic-NMR technique[**]; indeed DFT calculations predict a barrier of 29.0 kcal/mol. Additionally, the rotational process here corresponds to a topomerization hence there are no atropisomers to separate in this case. The two residual enantiomers due to the asymmetric carbon were separated by enantioselective HPLC on a Chiralcel AD-H column, to determine the absolute configuration by chirooptical methods. In particular, we used the theoretical calculation of the ECD spectra by means of the TD-DFT method, because this technique has emerged as a reliable approach to assign the absolute configuration, and it has been successfully used many times to predict the ECD spectra of complex organic molecules.[33–38]

The conformational search carried out by MM methods had shown that a second conformation, due to the rotation of the OH group, was available for each of the two conformational diastereoisomers. All the four resulting conformers are comprised in a 1 kcal/mol range, and the simulation of the ECD spectrum must take into account the contribution of all of them (Table 2). The electronic excitation energies and rotational strengths needed for the simulation of the ECD spectra have been calculated in the gas phase for the four conformations of **3** using TD-DFT with the 6-311++G(2d,p) basis set and the CAM-B3LYP[39] model. The rotational strengths were calculated with the dipole-length and the dipole-velocity gauge and the resulting values are very similar, the average difference being less than 3%. For this reason, the errors due to basis set incompleteness should be

TABLE 2. Calculated total energies (E°) and free energies (G°) of the conformations of 3 (in kcal/mol, CAM-B3LYP/6–31G(d) level)

Cpd.	Conformation[a]	E°	% Pop (ΔE°)	G°	% Pop (ΔG°)
3	*Syn*, 180	0.00	65	0.00	43
	Anti, 60	0.62	23	0.25	28
	Syn, 60	1.79	3	0.48	19
	Anti, 180	1.19	9	0.91	10

[a]The first descriptor correspond to the relationship between the OH and the CMe_2 group with respect to the plane of the aromatic ring of indane. The second descriptor indicates the dihedral angle of the hydroxyl hydrogen with respect to the mesityl quaternary carbon.
Populations percentages (Pop.) are calculated assuming Boltzmann statistics at $T = 25$°C.

[§]This is a "control" NOE effect that can be used as a distance marker for the calculation of the distance ratio with other moieties.

[¶]The calculated dihedral angle (Cq–Cq–Cq(OH)–CMe_2) is 23° in the case of **1** and −8° for **3**. This indicates that in the case of **3** the five membered ring is flatter and that in the best conformation of **3** the envelope is reversed (i.e. the OH and the CMe_2 are on the same side) with respect to **1**.

**At +140°C a rate constant of 10-20 Hz, corresponding to a barrier of 22 kcal/mol, would be clearly visible as a broadening of the two NMR lines.

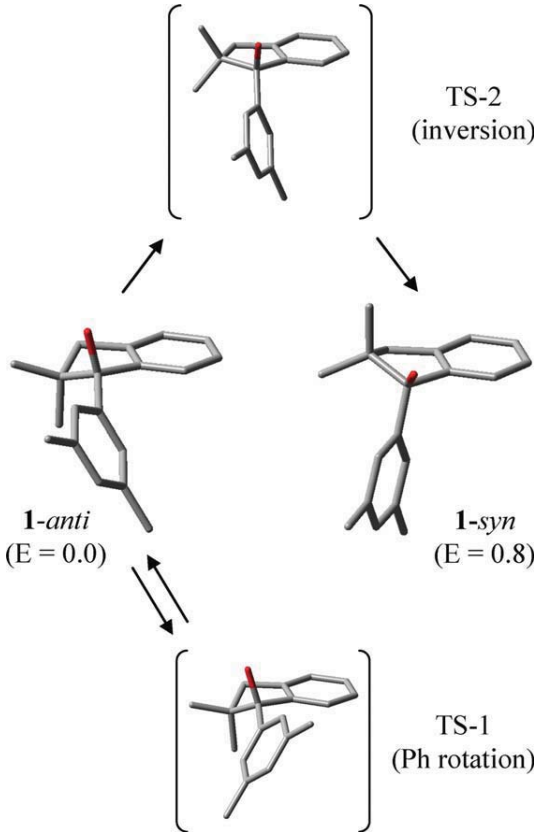

Fig. 3. Center: the two conformational diastereoisomers of **1**. Top: Calculated transitions state for the ring-flip process that interconverts the *anti* and *syn* diastereoisomers. Bottom: transition state for the rotation of 3,5-dimetylphenyl ring, corresponding to a topomerization process. [Color figure can be viewed in the online issue, which is available at wileyonlinelibrary.com.]

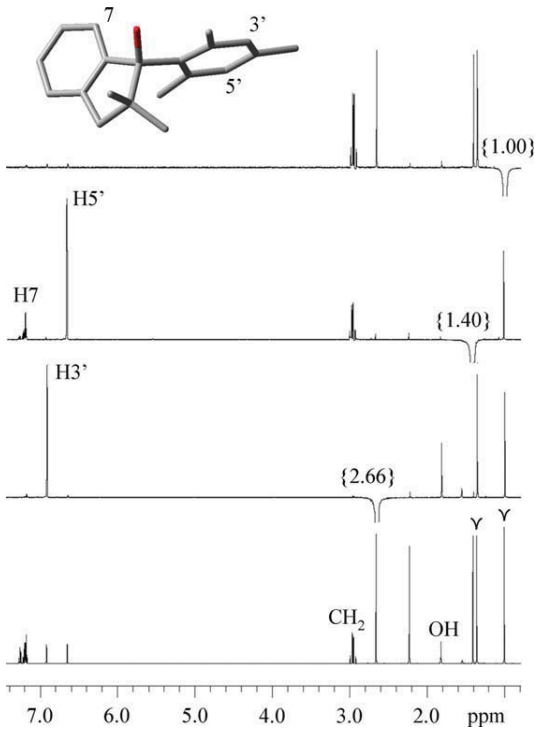

Fig. 4. NOE spectra (600 MHz in $CDCl_3$) of compound **3**. Bottom: control spectrum, the geminal methyls are marked with γ. Second and third traces: irradiation of the aromatic methyls at 2.66 and 1.40 ppm. Top: irradiation of the geminal methyl at 1.00 ppm. The 3D structure refers to the most stable conformation. [Color figure can be viewed in the online issue, which is available at wileyonlinelibrary.com.]

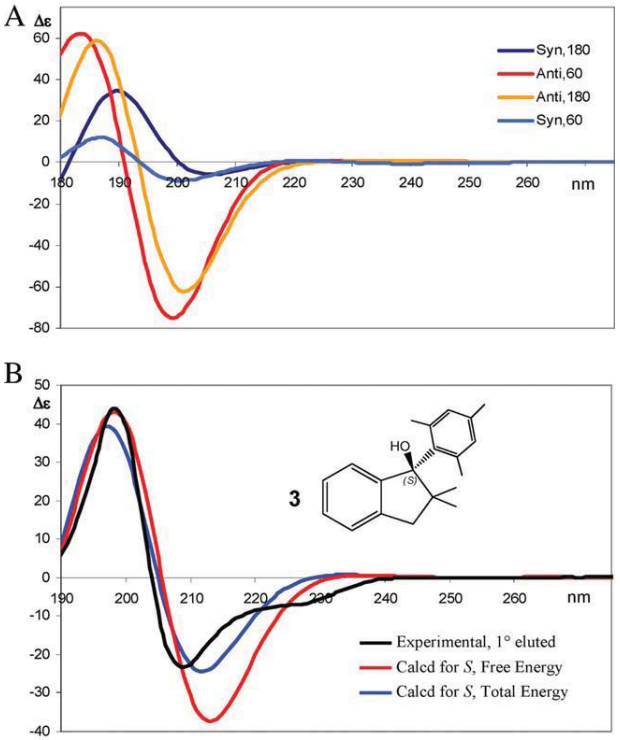

Fig. 5. A: calculated ECD spectra for the four conformation of **3**. Calculations were performed at the TD-DFT CAM-B3LYP/6-311++G(2d,p) level. B: experimental (black line, 1.1×10^{-4} M in acetonitrile) and calculated ECD spectra, weighed on the calculated free energies (ΔG°, red line) or on the total energies (Δ*E*°, blue line). Simulated spectra were redshifted by 10 nm and scaled to match the experimental trace. [Color figure can be viewed in the online issue, which is available at wileyonlinelibrary.com.]

very small, or negligible,[40] and the selected basis set should be considered suitable to tackle the present case. All the calculations were performed supposing the absolute configuration S, with the results shown in Figure 5. All the ECD spectra were generated by applying a 0.55 eV Gaussian shaped line width,[21] and to generate the spectrum in the 170–400 nm range, 60 transitions were calculated for each conformation.

The patterns of the simulated spectra for the four conformations are quite similar regarding the pattern, but quite different in the absolute intensity and in the relative intensity of the two Cotton effects. Therefore, any error in the exact determination of the conformer's population could noticeably influence the shape of the final spectrum. The final simulated ECD spectra were obtained taking into account the 43:28:19:10 or the 65:23:3:9 population ratios determined assuming Boltzmann statistics from the calculated free energies, or from the electronic total energies, at the CAM-B3LYP/6-31G(d) level, respectively (Table 2). In both cases, the agreement between the calculated and the experimental spectra obtained for the first eluted enantiomer is very good, and the ECD simulations suggest that the absolute configuration of this enantiomer of **3** is 1S. It should be noted that the spectral simulation obtained using the conformers ratio derived from the total energies is slightly better than that obtained from the ZPE-corrected energies.

To experimentally determine the rotational barrier of the mesityl and to achieve the separation of the stable atropisomers, the symmetry axis (C_{ipso}–C_{para}) was removed by inserting a methoxy group in the meta position (compound **4**). In the latter case, the molecule bears two chirality sources (i.e., the asymmetric carbon and a chirality axis) so that two diastereoisomers (each one corresponding to a pair of enan-

tiomers) are expected to exist: in one diastereoisomer (atropisomer), the OMe group is closer to the OH and the geminal methyls, whereas in the other, the OMe is far from OH and oriented inward the indanyl moiety. At ambient temperature, the ^{1}H and ^{13}C spectra of **4** show the presence of the two atropisomers in a 53:47 ratio.

The stereoisomeric mixture was separated at room temperature by means of a semipreparative enantioselective HPLC column (chiralcel AD-H, see Fig. S4 in the Supporting Information), but only three of the four expected stereoisomers could be achieved. The first and the third eluted peaks corresponded to the two enantiomers of the minor diastereoisomer (mesityl CH at 6.92 ppm), whereas the second peak corresponded to the major diastereoisomer (mesityl CH at 6.64 ppm), whose enantiomers were poorly separated. This pair of enantiomers was eventually resolved using a different enantioselective column (Phenomenex LUX Amylose-2). The absence of any effect due to in-column interconversion in the chromatograms confirmed that the rotational barrier of the mesithyl group is larger than 23 kcal/mol.[41–46]

NOE experiments taken on the major atropisomer showed that the irradiation of the *ortho*-methyl at 1.29 ppm resulted in a strong enhancement on the adjacent hydrogen of the ring and in weaker NOE effects on the H7 and CH_2 of the indanyl moiety. Conversely, the irradiation of the *ortho*-methyl at 2.54 ppm showed a strong NOE effect on the adjacent OMe, marked enhancements on the OH and both the geminal methyls of the indane, confirming that in the major atropisomer the OMe is spatially close to the OH (Fig. S5, Supporting Information). From an alternative point of view, the major atropisomer corresponds to a syn-periplanar (sp) disposition of the OH group with respect to the methoxymesityl.[1,47] Taking into account the dihedral angle ($Ar_{indanyl}$)C–C1–C_{ipso}–C_{ortho}(OMe side), the R*,M* relative configuration can be assigned to the major atropisomer (see Fig. S6, Supporting Information).

Following the same approach already shown for compound **3**, the experimental ECD spectra of a pure enantiomer was acquired in acetonitrile and simulated by the TD-DFT method. In the case of compound **4**, the results of NOE analysis helped in the assignment of the absolute configuration, in that the relative configuration was already assigned.

The minor diastereoisomer had been determined to have the R*,P* configuration, and the ECD spectrum of the second eluted enantiomer (Fig. 6, third peak on the AD-H column) was correctly simulated by the calculations taken on the R,P enantiomer (see Figs. S6 and S7 and Table S1 of the Supporting Information for tables and spectra of the populated conformations). This assignment is further supported by the comparison with the spectrum of the S enantiomer of compound **3** that exhibits the mirror image spectrum. The correspondence with the two peaks observed on the LUX column for the major diastereoisomer was determined by the kinetic equilibration of the R,P enantiomer into the R,P/R,M mixture, because during this equilibration, the rotation of the methoxymesityl group selectively causes the helicity change of the chirality axis. When subjected to HPLC analysis, the R,M atropisomer (major) showed to be the first eluted on the LUX column. Consequently, the second eluted enantiomer had to be the S,M atropisomer.

The rotational barrier of the 3-methoxy-mesityl moiety could be determined by heating at +80°C an NMR sample of the most retained enantiomer and following the equilibration into the more stable atropisomer (k_1; Fig. S8, Supporting Information). A classic kinetic treatment gave a rate constant (k_2) of 1.5×10^{-4} s^{-1} for the conversion of the more into the less stable atropisomer to which corresponds a rotational barrier of 26.9_5 kcal/mol that is in good agreement with the calculated value.

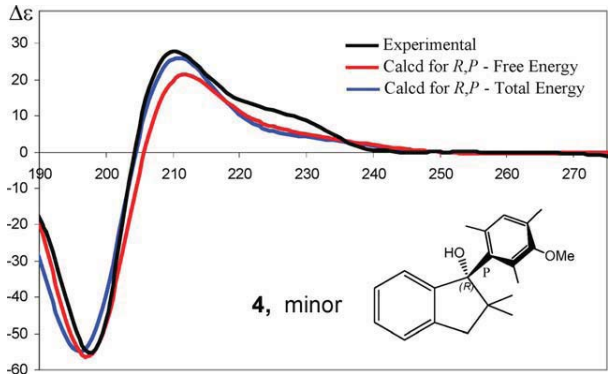

Fig. 6. Experimental (black line, 1.2×10^{-4} M in acetonitrile) and calculated ECD spectra, weighed on the calculated free energies (ΔG°, red line) or on the total energies (ΔE°, blue line) of the 2° eluted enantiomer of the minor atropisomer of **4** (on AD-H column). Calculations were performed at the TD-DFT CAM-B3LYP/6-311++G(2d,p) level. Simulated spectra were redshifted by 10 nm and scaled to match the experimental trace. [Color figure can be viewed in the online issue, which is available at wileyonlinelibrary.com.]

Likewise compound **6**, where the aryl substituent is the 1-naphthyl, lacks any element of symmetry coincident with the rotational axis and, as for **4**, the presence of two stable atropisomers at room temperature is highlighted by two sets of signals in a 89:11 ratio.

NOE experiments on the signals of the major atropisomer (Fig. S9, Supporting Information) showed that irradiation of the methyl at 0.67 ppm yielded a marked enhancement on the doublet at 6.63 ppm attributed to H2′ of the naphthyl moiety, whereas the irradiation of the methyl at 1.31 ppm yields NOE effects on the OH at 3.97 ppm and on the doublet at 9.26 ppm, assigned to the H8′ of the naphthalene (peri hydrogen). Conversely, when the OH signal is saturated, NOE effects were observed on the signals at 1.31, 9.26, and 7.30 ppm, the latter being assigned to the peri hydrogen (H7) of the indanyl moiety. Finally, the irradiation of H8′ at 9.26 ppm that produces NOE effects on the OH and on both the geminal methyls corroborate a geometry where the naphthyl moiety has the H2′ placed above the indanyl ring and points inward the molecule, whereas the H8′ is located under the indanyl, close to the OH and the geminal methyl at 1.31 ppm. From an alternative point of view, the major atropisomer corresponds to a syn-periplanar (sp) disposition of the OH group with respect to naphthalene (see Fig. 7).

The X-ray structure of **6** (crystals grown from *n*-hexane, see Fig. 7 and Supporting Information Fig. S10) confirms that in the solid state the preferred conformation corresponds to the most populated atropisomer in solution. The naphthyl and indanyl rings are nearly perpendicular, as the dihedral angle C2—C1—C1′—C2′ is 93.7°. The H2′ is located above the indanyl ring at a distance of 3.39 Å from H7 and H8′, only 2.27 Å away from OH, and 2.39Å from the closest hydrogen of the geminal methyl under the indanyl ring. The shape of the five-membered ring corresponds to an

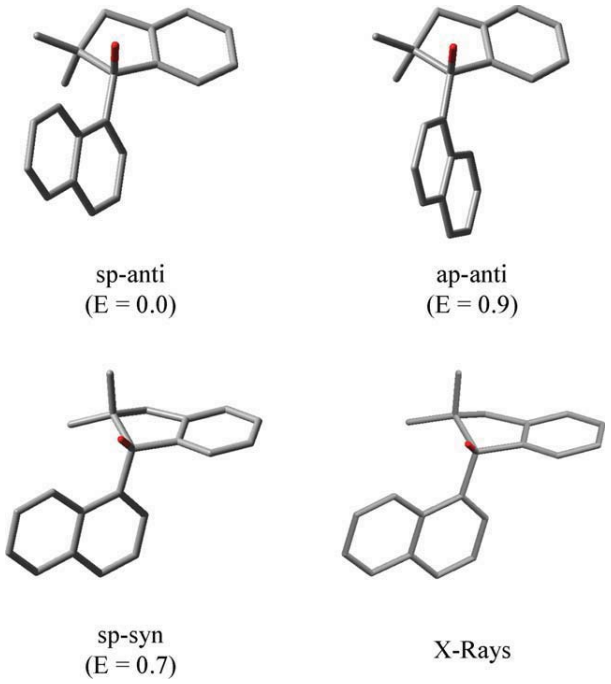

Fig. 7. Calculated conformational diastereoisomers of **6** and experimental X-ray structure. [Color figure can be viewed in the online issue, which is available at wileyonlinelibrary.com.]

envelope in which the CMe_2 is out of the plane of the phenyl by 21.8° (Cq–Cq–CH_2–CMe_2 dihedral angle) and on the same side of the OH (thus sp-*syn*). This shape was correctly simulated by the calculations in the case of compound **1**, where two conformations, resulting from the frozen inversion of the cycle, were detected. This is a further confirmation of the accuracy and reliability of the DFT approach. Taking into account the rotational asymmetry of naphthalene and the two available dispositions of the five-membered ring, a total of four conformational diastereoisomers can be envisaged (sp-*syn*, sp-*anti*, ap-*syn*, ap-*anti*).

DFT calculations show that the conformation derived by the NOE experiments, with the OH group close to H8′ is the most stable. The other conformation, due to 180° rotation of the naphthalene (OH close to H2′, antiperiplanar), is calculated to be 0.9 kcal/mol less stable, in good agreement with the experimental ratio (see Table 1). The calculations also suggest that the best conformation of the syn-periplanar (sp) atropisomer is sp-*anti* (see Fig. 7) and this does not correspond to that observed in the solid state. The latter conformation (sp-*syn*) has a calculated energy of 0.7 kcal/mol higher that the former (see also Fig. S10 in the Supporting Information). This mismatch is probably due to the constraints imposed by the crystal lattice. However, it is impossible to derive from the NOE data whether the most populated conformation in solution corresponds to the X-ray conformation or to the calculated one. Both conformations are probably populated and the very fast ring inversion implies the observation of averaged NOEs effects. For this reason, the saturation of H8′ at 9.26 ppm yields identical NOE enhancements on both the geminal methyls of indane (top trace in Fig. S9, Supporting Information).[††]

[††]These enhancements should be quite different if only one of the two conformations were populated.

The calculations indicate that also in the case of the antiperiplanar (ap) atropisomer, where the OH is close to H2′, the CMe_2 group is far from the OH (ap-*anti*); whereas the remaining conformation, in which the envelope is reversed (ap-*syn*) and has a much higher energy (3.5 kcal/mol). When a sample of **6** is heated, all the NMR signals broaden and eventually coalesce in the range 85–100°C, yielding sharp single signals above 140°C. From the line shape simulation of the CH_2 signal, an activation energy of 18.8 kcal/mol (Fig. 8) was derived.

Two pathways are possible for the rotation about the pivotal C1—C1′ bond that allows the interconversion between the two atropisomers, namely the crossing of H8′ or H2′ over the geminal methyls. DFT calculations indicate that the first path is higher in energy (26.5 kcal/mol) due to the greater distortion of the indanyl ring required to allow the leapfrogging of the methyl. Instead, the crossing of H2′ over the geminal methyl needs a maximum energy of 19.6 kcal/mol even if the H8′, at the same time, has to climb over H7 in the indanyl plane. It has to be noted that the lower calculated barrier (i.e., the threshold transition state for the rotation of naphthalene) is actually very close to the experimental value.

The same conformational behavior was also observed in compound **5**, where the naphthyl is replaced by the 7-benzothiophene. NOE experiments (Fig. S11, Supporting Information) corroborate the hypothesis that the most populated conformation is the same as for **6** (i.e., sp). In addition to that the presence of a five-membered ring and the sulphur atom in the peri position reduce the steric clashing in the transition state, thus a smaller barrier is expected to occur. ^{1}H NMR spectra of **5** at variable temperature showed at +38°C, the maximum broadening for the methyl at 1.31 ppm and this allowed to estimate a rotational barrier of 16.7 kcal/mol. Furthermore, on cooling at −30°C, the same methyl signal

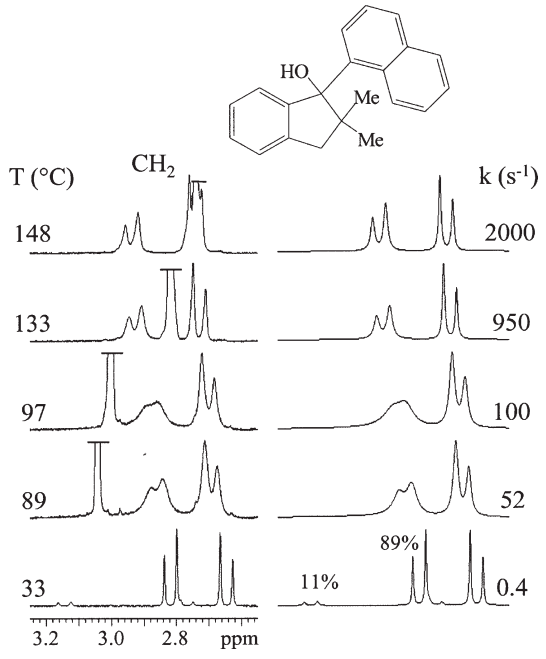

Fig. 8. ^{1}H NMR spectra (600 MHz in DMSO-d_6) of compound **6**. Left: experimental traces at different temperatures referring to the indanyl CH_2. Right: simulated traces and calculated rate constants (*k*) at the same temperatures.

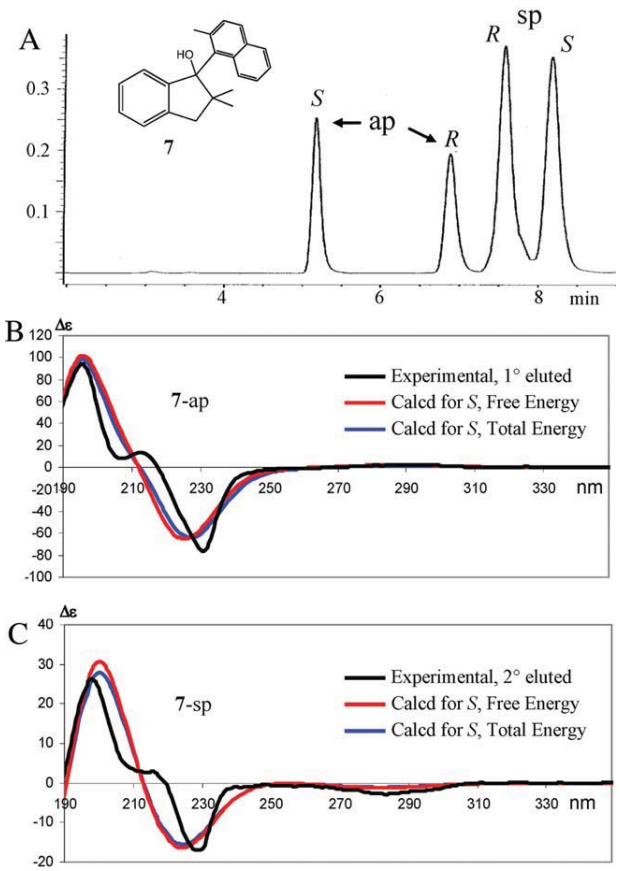

Fig. 9. A: Enantioselective HPLC trace of compound **7** on Chiralcel AD-H (eluent: hexane/iPrOH 90:10 v/v). B: Experimental (black line, 1.0×10^{-4} M in acetonitrile) and calculated ECD spectra for the first eluted enantiomer of the minor atropisomer. C: Experimental (black line, 1.2×10^{-4} M in acetonitrile) and calculated ECD spectra for the second eluted enantiomer of the major atropisomer (fourth peak). The red lines correspond to the simulation weighed on the calculated free energies (ΔG°), blue lines correspond to the simulations weighed on the calculated total energies (ΔE°). Simulated spectra were redshifted by 10 nm and multiplied by 1.1 in order to match the experimental trace. [Color figure can be viewed in the online issue, which is available at wileyonlinelibrary.com.]

sharpens and a partner peak (population 4%) appears at a lower frequency with a separation of 43 Hz (Fig. S12, Supporting Information). Most likely, such a large difference between the two atropisomer populations could be due to an hydrogen bonding interaction between the OH and the sulphur atom that favors the sp-atropisomer.

Similar to compounds **1** and **3**, when the H2′ of the naphthyl moiety is replaced by a methyl, as in compounds **7**, a larger rotational barrier is expected, because the methyl is again forced to pass over the indanyl moiety. Indeed, ^{1}H and ^{13}C NMR spectra of **7** at room temperature show two groups of signals in a 70:30 ratio corresponding to the two stable atropisomers. Unlike **4**, the expected pair of enantiomers for each diastereoisomer, in the ratio estimated by NMR, have been nicely separated by enantioselective HPLC on a semipreparative chiralcel AD-H column eluted with *n*-hexane/ isopropyl alcohol 95:5 (Fig. 9).

NOE experiments on the major atropisomer of **7** show that irradiation of the OH at 5.53 ppm yields enhancements on the H7 at 7.30 ppm, on the methyl at 1.40 ppm and the H8′ of the naphthyl ring at 9.16 ppm. Conversely, irradiation of the Me at 0.91 ppm give NOE effects only on the CH_2 at 2.92 ppm, the geminal methyl at 1.40 ppm and the 2-Me of the naphthyl at 1.50 ppm (Fig. S13, Supporting Information). This suggests a preferred conformation in which the naphthyl is turned nearly orthogonal to the indanyl ring and the 2-Me group, on the opposite side of the OH (thus syn-periplanar). Taking into account the dihedral angle between the naphthyl ring and the indane, the syn-periplanar pair of enantiomers has the R*,M* relative configuration, whereas the anti-periplanar pair has the R*,P* relative configuration. DFT calculations indicate the syn-periplanar atropisomer to be more stable than the anti-periplanar by 0.4 kcal/mol (after ZPE correction), in good agreement with the experimental value (0.5 kcal/mol). The rotational barrier of the 2-methylnaphtyl was determined at +70°C on the first eluted peak of the minor atropisomer by a classical kinetic equilibration in DMSO-d_6, from the less to the more stable atropisomer (Fig. S14, Supporting Information). A rate constant (k_1) of 4.0×10^{-4} s^{-1} was obtained, corresponding to a rotational barrier of 25.5 kcal/mol that turned out to be in good agreement with the DFT calculated value (26.7 kcal/mol).

As in the cases of compounds **3** and **4**, the absolute configuration of the atropisomers of **7** was determined by the simulation of the ECD spectra. For each atropisomer, the two different conformations of the five-membered ring and the two orientations of the OH had to be considered, yielding a total of 8 stereoisomers (see Table S2 in the Supporting Information). DFT optimization (B3LYP/6-31G(d) level) of each stereoisomer suggested that all of them had to be considered in the simulation of the ECD spectrum.

The electronic excitation energies and rotational strengths were calculated in the gas phase for the four conformations of **7**-ap and **7**-sp using TD-DFT with the 6-311++G(2d,p) basis set and the CAM-B3LYP model. All the calculations were performed supposing the S absolute configuration, and all the ECD spectra were generated by applying a 0.55 eV Gaussian shaped line width.[21] To generate the spectrum in the 170–400 nm range, 75 transitions were calculated for each conformation (see Fig. S15 of the Supporting Information for the calculated ECD spectrum of each conformation). The final simulated ECD spectra (Fig. 9) were obtained taking into account the population ratios determined assuming Boltzmann statistics from the calculated free energies or from the electronic total energies (Table S2 of the Supporting Information).

CONCLUSIONS

For the investigated 1-arylindanols (**1–7**), we have shown that the barrier involved in the rotational process about the pivotal bond C1(indanyl)—C1′ (aryl) cover the wide range 10–26 kcal/mol, and such results are strongly dependent on the hindrance of the aryl and the indanyl moieties. When the *ortho*-aryl hydrogens are replaced with methyls, the rotational process is already locked at room temperature. Furthermore, if the rotational axis is not coincident with the local symmetry axis of the aryl moiety two diastereoisomers are generated, each one as a pair of enantiomers, because of the chiral center on the indane framework. In the cases of **4** and **7**, all the four stereoisomers have been separated by enantioselective HPLC and their relative molecular geometries have been assigned by NMR, as well as the rotational barriers for their interconversion were determined by kinetic equilibration. These results were further corroborated from detailed

computations of the ground and transition states. These enabled the calculation of the rotational barriers and the simulation ECD spectra, from which the absolute configuration of each stereoisomer could be reliably assigned.

ACKNOWLEDGMENTS

The authors thank Prof. L. Lunazzi for reading the manuscript and to CIGAS, University of Basilicata, for running the ESI-HRMS analyses.

LITERATURE CITED

1. Casarini D, Lunazzi L, Mazzanti A, Foresti E. Conformational studies by dynamic NMR. 64. Stereomutations of atropisomers and of conformational enantiomers in ethers of hindered naphthylcarbinols. J Org Chem 1998;63:4746–4754.
2. Casarini D, Coluccini C, Lunazzi L, Mazzanti A. Stereolabile and configurationally stable atropisomers of hindered aryl carbinols. J Org Chem 2005;70:5098–5102.
3. Casarini D, Lunazzi L, Mazzanti A, Mancinelli M. Conformation and stereodynamics of symmetrically *ortho*-disubstituted aryl carbinols and aryl ethers. J Org Chem 2007;72:998–1004.
4. Casarini D, Lunazzi L, Mazzanti A, Mancinelli M. Structure, conformations, stereodynamics, dimer formation and absolute configuration of axially chiral atropisomers of hindered biphenyl carbinols. J Org Chem 2007;72:7667–7676.
5. Cheer JC, Johonson CR. The stereoselective rearrangements of conformationally mobile epoxides. J Am Chem Soc 1968;90:178–183.
6. Palmer M, Walsgrove T, Wills M. (1R,2S)-(+)-cis-1-Amino-2-indanol: an effective ligand for asymmetric catalysis of transfer hydrogenations of ketones. J Org Chem 1997;62:5226–5228.
7. Brewster JH, Buta JG. Conformational mobility and optical rotation effects of aromatic nuclei. J Am Chem Soc 1966;88:2233–2240.
8. Al-Saadi AA, Wagner M, Laane J. Spectroscopic and computational studies of the intramolecular hydrogen bonding of 2-indanol. J Phys Chem A 2006;110:12292–12297.
9. Pincock JA, Wedge PJ. The photochemistry of conformationally rigid benzilic esters:2,2-dimethyl-1-indanyl acetates and pivalates. J Org Chem 1995;60:4067–4076.
10. Orliac-le Moing A, Delauny J, LeBouc A, Simonet J. Reduction electrochimique des derives carbonyles insatures. IX. Indanones et tetralones: electrolyses mixtes en presence d'electrophiles. Tetrahedron 1985;41:4483–4493.
11. Fuson RC, Corse J, Welldon PB. Enediols. VIII. Methoxystilbenediols J Org Chem 1941;63:2645–2648.
12. Bradley SA, Krishnamurthy K. A modified CRISIS-HSQC for band-selective IMPRESS. Magn Res Chem 2005;43:117–123.
13. Willker W, Leibfritz D, Kerssebaum R, Bermel W. Gradient selection in inverse heteronuclear correlation spectroscopy. Magn Res Chem 1993;31:287–292.
14. Hurd RE, John BK. Gradient-enhanced proton-detected heteronuclear multiple-quantum coherence spectroscopy. J Magn Reson 1991;91:648–653.
15. Stott K, Stonehouse J, Keeler J, Hwand TL, Shaka AJ. Excitation sculpting in high-resolution nuclear magnetic resonance spectroscopy: Application to selective NOE experiments. J Am Chem Soc 1995;117:4199–4200.
16. Kupče E, Boyd J, Campbell ID. Short selective pulses for biochemical applications. J Magn Reson Series B 1995;106:300–303.
17. Frisch MJ, Trucks GW, Schlegel HB, Scuseria GE, Robb MA, Cheeseman JR, Montgomery JA, Jr, Vreven T, Kudin KN, Burant JC, Millam JM, Iyengar SS, Tomasi J, Barone V, Mennucci B, Cossi M, Scalmani G, Rega N, Petersson GA, Nakatsuji H, Hada M, Ehara M, Toyota K, Fukuda R, Hasegawa J, Ishida M, Nakajima T, Honda Y, Kitao O, Nakai H, Klene M, Li X, Knox JE, Hratchian HP, Cross JB, Bakken V, Adamo C, Jaramillo J, Gomperts R, Stratmann RE, Yazyev O, Austin AJ, Cammi R, Pomelli C, Ochterski JW, Ayala PY, Morokuma K, Voth GA, Salvador P, Dannenberg JJ, Zakrzewski VG, Dapprich S, Daniels AD, Strain MC, Farkas ,O, Malick DK, Rabuck AD, Raghavachari K, Foresman JB, Ortiz JV, Cui Q, Baboul AG, Clifford S, Cioslowski J, Stefanov BB, Liu G, Liashenko A, Piskorz P, Komaromi I, Martin RL, Fox DJ, Keith T, Al-Laham MA, Peng CY, Nanayakkara A, Challacombe M, Gill PMW, Johnson B, Chen W, Wong MW, Gonzalez C, Pople JA. Gaussian 03, Revision D.01. Wallingford CT: Gaussian, Inc.; 2005.
18. Frisch M J, Trucks GW, Schlegel HB, Scuseria GE, Robb MA, Cheeseman JR, Scalmani G, Barone V, Mennucci B, Petersson GA, Nakatsuji H, Caricato M, Li X, Hratchian HP, Izmaylov AF, Bloino J, Zheng G, Sonnenberg JL, Hada M, Ehara M, Toyota K, Fukuda R, Hasegawa J, Ishida M, Nakajima T, Honda Y, Kitao O, Nakai H, Vreven T, Montgomery JA, Jr, Peralta JE, Ogliaro F, Bearpark M, Heyd JJ, Brothers E, Kudin KN, Staroverov VN, Kobayashi R, Normand J, Raghavachari K, Rendell A, Burant JC, Iyengar SS, Tomasi J, Cossi M, Rega N, Millam NJ, Klene M. Knox JE, Cross JB, Bakken V, Adamo C, Jaramillo J, Gomperts R, Stratmann RE, Yazyev O, Austin AJ, Cammi R, Pomelli C, Ochterski JW, Martin RL, Morokuma K, Zakrzewski VG, Voth GA, Salvador P, Dannenberg JJ, Dapprich S, Daniels AD, Farkas Ö, Foresman JB, Ortiz JV, Cioslowski J, Fox DJ. Gaussian 09, Revision A.1. Wallingford, CT: Gaussian, Inc., 2009.
19. Ayala PY, Schlegel HB. Identification and treatment of internal rotation in normal mode vibrational analysis. J Chem Phys 1998;108:2314–2325.
20. Casarini D, Lunazzi L, Mazzanti A. Recent advances in stereodynamics and conformational analysis by dynamic NMR spectroscopy and theoretical calculations. Eur J Org Chem 2010;2035–2056.
21. Donnington RD, Keith TA, Millam JM. Gaussview 5.0.9, Semichem, 2008.
22. Lomas JS, Luong PK, Dubois JE. Nucleophilic addition of *o*-tolyllithium compounds to di-*tert*-butyl ketone. Thermal and organolithium-catalyzed isomerization of *o*-tolyldi-*tert*-butylcarbinol rotamers. J Org Chem 1977;42:3394–3399.
23. Lomas JS, Anderson JE. Synthesis and very slow sp^2-sp^3 rotation of anti-*o*-tolyldi(1-adamantyl)methane. J Org Chem 1995;60:3246–3248.
24. Jennings WB. Chemical shift nonequivalence in prochiral groups. Chem Rev 1975;75:307–322.
25. Casarini D, Lunazzi L, Mazzanti A. Correlated rotations in benzylfluorene derivatives: structure, conformation and stereodynamics. J Org Chem 2007;73:2811–2818.
26. Casarini D, Lunazzi L, Mazzanti A. Steric effects which determine the conformational preferences and stereodynamic processes of aryl fluorenyl ketones. Org. Biomol Chem 2009;7:1619–1626.
27. Grilli S, Lunazzi L, Mazzanti A, Casarini D, Femoni C. Conformational studies by dynamic NMR. 78. Stereomutation of the helical enantiomers of trigonal carbon diaryl-substituted compounds: dimesitylketone, -thioketone and -ethylene. J Org Chem 2001;66:488–495.
28. Mislow K. Stereochemical consequences of correlated rotation in molecular propellers. Acc Chem Res 1976;9:26–33.
29. Mazzanti A, Lunazzi L, Ruzziconi R, Spizzichino S, Schlosser M. The torsional barriers of 2-hydroxy- and 2-fluorobiphenyl: small, but measurable. Chem Eur J 2010;16:9186–9192.
30. Anet FAL, Chmurni GN, Krane J. Ring inversion in cyclohexanone. J Am Chem Soc 1973;95:4423–4424.
31. Pawar DM, Miggins SD, Smith SV, Noe EA. Conformational study of *cis*-cyclononene by dynamic NMR spectroscopy and computational methods. J Org Chem 1999;64:2418–2421.
32. Casarini D, Grilli S, Lunazzi L, Mazzanti A. Conformational studies by dynamic NMR. 80. Cog-Wheel effect in the stereolabile helical enantiomers of dimesityl sulfoxide and sulfone. J Org Chem 2001;66:2757–2763.
33. Bringmann G, Bruhn T, Maksimenka K, Hemberger Y. The assignment of absolute stereostructures through quantum chemical circular dichroism calculations. Eur J Org Chem 2009:2717–2727.
34. Stephens PJ, Pan JJ, Devlin FJ, Krohn K, Kurtán K. Determination of the absolute configurations of natural products via density functional theory calculations of vibrational circular dichroism, electronic circular dichroism, and optical rotation: The iridoids plumericin and isoplumericin. J Org Chem 2007;72:3521–3536.
35. Kwit M, Rozwadowska MD, Gawroński J, Grajewska A. Density functional theory calculations of the optical rotation and electronic circular dichroism: The absolute configuration of the highly flexible *trans*-isocytoxazone revised. J Org Chem 2009;74:8051–8063.
36. Gioia C, Fini F, Mazzanti A, Bernardi L, Ricci A. Organocatalytic asymmetric formal [3 + 2] cycloaddition with in situ-generated *N*-carbamoyl nitrones J Am Chem Soc 2009;131:9614–9615.

37. Pescitelli G, Di Pietro S, Cardellicchio C, Annunziata M, Capozzi M, Di Bari L. Systematic investigation of CD spectra of aryl benzyl sulfoxides interpreted by means of TDDFT calculations. J Org Chem 2010;75:1143–1154.
38. Bencivenni G, Wu L-Y, Giannichi B, Mazzanti A, Pesciaioli F, Song M-P, Bartoli G, Melchiorre P. Targeting structural and stereochemical complexity by asymmetric organocascade: construction of spirocyclic oxindoles having multiple stereocenters. Angew Chem Int Ed Engl 2009;48:7200–7203.
39. Yanai T, Tew D, Handy N. A new hybrid exchange–correlation functional using the Coulomb-attenuating method (CAM-B3LYP). Chem Phys Lett 2004;393:51–57.
40. Stephens PJ, McCann DM, Devlin FJ, Cheeseman JR, Frisch MJ. Determination of the absolute configuration of [3_2](1,4)barrelenophanedicarbonitrile using concerted time-dependent density functional theory calculations of optical rotation and electronic circular dichroism. J Am Chem Soc 2004;126:7514–7521.
41. D'Acquarica I, Gasparrini F, Pierini M, Villani C, Zappia G. Dynamic HPLC on chiral stationary phases: a powerful tool for the investigation of stereomutation processes. J Sep Sci 2006;29:1508–1516.
42. Trapp O. unified equation for access to rate constants of first-order reactions in dynamic and on-column reaction chromatography. Anal Chem 2006;78:189–198.
43. Wolf C. Stereolabile chiral compounds: analysis by dynamic chromatography and stopped-flow methods. Chem Soc Rev 2005;34:595–608.
44. Trapp O, Shellie R, Marriott P, Schurig V. Simulation of elution profiles for two-dimensional dynamic gas chromatographic experiments. Anal Chem 2003;75:4452–4461.
45. Trapp O, Schurig V. Stereointegrity of Tröger's base: gas-chromatographic determination of the enantiomerization barrier. J Am Chem Soc 2000;122:1424–1430.
46. Alcaro S, Casarini D, Gasparrini F, Lunazzi L, Villani C. Atropisomerism in hindered naphthyl sulfones investigated by dynamic NMR and dynamic HPLC techniques. J Org Chem 1995;60:5515–5519.
47. Casarini D, Lunazzi L, Mazzanti A. Conformational studies by dynamic nuclear magnetic resonance. Part 59. Stereodynamics of conformational enantiomers in the atropisomers of hindered naphthilcarbinols. J Org Chem 1997;62:3315–3323.